Journal of Power Sources 196 (2011) 2725–2734

Contents lists available at ScienceDirect

Journal of Power Sources

journal homepage: www.elsevier.com/locate/jpowsour

Analysis of liquid water transport in fuel cell gas diffusion media using two-mobile phase pore network simulations

B. Markicevic, N. Djilali*

Institute for Integrated Energy Systems and Department of Mechanical Engineering, University of Victoria, Victoria, BC V8W 3P6, Canada

ARTICLE INFO

Article history:
Received 15 September 2010
Received in revised form 2 November 2010
Accepted 3 November 2010
Available online 10 November 2010

Keywords:
Gas diffusion layer
Porous media
Two phase flow
Relative permeability
Capillary function
PEM fuel cell

ABSTRACT

Transport of liquid water in a fuel cell gas diffusion layer is analyzed using capillary network modeling in which the mobility of both liquid and gas phases is considered to examine two distinct multiphase flow regimes: displacement and co-current flows. The simulations utilize a modified invasion percolation with trapping algorithm, and the capillary network consists of throats of different radii to account for the local heterogeneities of the porous media. Both displacement and two-mobile phase flow are solved, with inlet boundary condition for two-mobile phase flow prescribed through a discrete sequence of alternating phases entering the network. For both flow types (displacement and two-mobile phase), the cases studied range from capillary force controlled, where the maximum distance between two throats filled consecutively is equal to the network size, to viscous force controlled, where the maximum distance is set so as not to exceed some predefined value that is less than the network size. The maximum distance determines the distribution of phases; phase entrapment, percolation, and channeling are observed during the spread of phases for distinct flow conditions. Once a distribution of phases is obtained, we calculate saturation, relative permeabilities, and the capillary pressure at the interface between the phases; we also determine the dependence of these transport parameters on medium heterogeneity and cluster size. Finally, the changes of relative permeability and capillary pressure as a function of saturation are compared for displacement and two-mobile phase flow.

1. Introduction

Water plays a critical role in the operation of PEM fuel cells. In order to achieve models that are physically representative of the multiphase flow nature of water transport in gas diffusion layers (GDLs), two issues need to be resolved. The first is understanding of the water flow mechanisms, when liquid water displaces the gas phase, or when gas and liquid phase flow co-currently through the GDL. The second is the prediction of the multiphase transport parameters for a given flow mechanism. Two additional transport processes need to be kept in mind: water evaporation and capillary flow, which can greatly influence the liquid water flow pattern [1,2]. MRI experimental results [3] for sessile droplets show that the evolution of imbibed liquids can differ significantly depending on the relative magnitude of evaporation and capillary flow rates.

Once the water transport mechanism is defined, the liquid water distribution can be obtained by solving the multiphase conservation equations [4,5]. It is generally accepted that the capillary pressure can be expressed using the Leverett *J*-function [6,7] and the relative permeability changes as a power law of the saturation [8,9], and this is the basis of most macroscopic fuel cell models accounting for liquid water transport in the GDL. Although the definitive form of relations specifically applicable to the fibrous hydrophobic GDL media remains to be established, some notable progress in this direction has been made recently [10,11]. The parameters that influence the relative permeability power law are discussed and summarized by Valavanides and Payatakes [12], where the value of the exponent changes due to the difference in length scales of the porous medium and distributed phase(s) [13,14] that may be caused by medium structure or process dynamics [15].

The dependencies between different scales can be elucidated by using capillary network models [16] in which the porous medium is represented as a network of pores and throats. Three different forces – capillary, viscous and gravitational – govern the multiphase flow [17,18], and their relative influence on the multiphase flow is quantified by the capillary and Bond numbers. For very slow flow (small capillary number) and negligible gravity, the flow is dominated by capillary forces [19]. It has been shown [20] that slow, non-wetting liquid displacement flows follow the invasion percolation process. This percolation problem has been formulated by Wilkinson and Willemsen [21], whereby the interface advances at each discrete step only at one point in which the potential threshold is satisfied. For a wetting liquid, or higher capillary numbers,

* Corresponding author. Tel.: +1 250 721 6034; fax: +1 250 721 6323.
E-mail address: ndjilali@uvic.ca (N. Djilali).

0378-7753/$ – see front matter © 2010 Elsevier B.V. All rights reserved.
doi:10.1016/j.jpowsour.2010.11.008

dynamic schemes [22] need to be used. In this case, for one discrete step, more than one point at the interface can satisfy the potential threshold, and each pore can be filled/emptied more than once during the flow process.

The fuel cell gas diffusion layer is an inherently heterogeneous fibrous porous medium [10] in which liquid water is distributed to form percolating flow paths. Using the percolation algorithm, a network structure which represents a GDL can be defined to match experimental capillary pressure curves of some actual GDLs [23]. The changes of the relative permeability and capillary pressure in the limit of capillary flow as predicted from the invasion percolation are reported by Markicevic et al. [24], where this algorithm was used to investigate directed water transport [25]. Nam and Kaviany [26] have used network simulations to establish how the diffusion coefficient depends on the saturation, using a cubic law for the relative permeability and a *J*-function for capillary pressure in the momentum transport equation. Network models reveal [27] that both geometrical and capillary properties influence the liquid water distribution in the GDL. Experimental evidence [28–30] shows that liquid water clusters throughout the GDL; thus, water emerges in specific points in the channel area rather than flow continuously across the overall available interface between the GDL and the channel. Based on the cluster size, the correlation length of the liquid water flow can be calculated, where recently it has been shown [31] that the GDL thickness is smaller than the correlation length which limits the use of continuum models.

In this study, co-current flow of two mobile phases is investigated and the impact of variations of flow rates of both phases at the inlet of the porous medium, of the maximum allowable cluster size (correlation length), and of the heterogeneity of the porous medium are examined. For the limiting case when one of the phases at the inlet boundary is dominant, the co-current flow reverts to displacement flow. For the spread of both phases, invasion percolation with trapping is used, whereby both phases form static structures and momentum transfer between the phases is negligible. The trapping rule is altered so that it can account for the presence of two mobile phases. Furthermore, the invasion percolation algorithm is modified for variable correlation length, in which the width of the advancing interface cannot exceed a predefined correlation length. The invasion is stopped at the termination point, when all throats at the outlet boundary are invaded by one of the phases transported from the network inlet. Based on the resulting patterns, the relative permeability of each phase as well as the capillary pressure at the interface are calculated and the impact of saturation and other investigated parameters is analyzed.

2. Model system

A discrete capillary network model for two-phase flow in which both phases are mobile is developed. The network consists of throats and pores, where the network coordination number represents the number of pores connected to one pore. For regular, square networks, the network coordination number is constant and equal to four. A schematic of the network and definitions of the parameters are shown in Fig. 1. In the network, each throat can only be occupied by one phase. Both phases enter the network at the inlet boundary and in order to vary their flow rates, the number of invading steps of the first (n_1) and second phase (n_2) is prescribed (*e.g.* when $n_1 = 1$ and $n_2 = 2$, for each throat invaded by the first phase, two throats are invaded by second phase). Hence, the occurrence frequency is defined as a ratio of invading steps ($\nu = n_1/n_2$), and either phase can be dominant compared to the other. The process repeats alternatively until there are no more available throats to occupy; this corresponds to the termination point. Once the flow paths of the phases are initiated, they branch into the porous

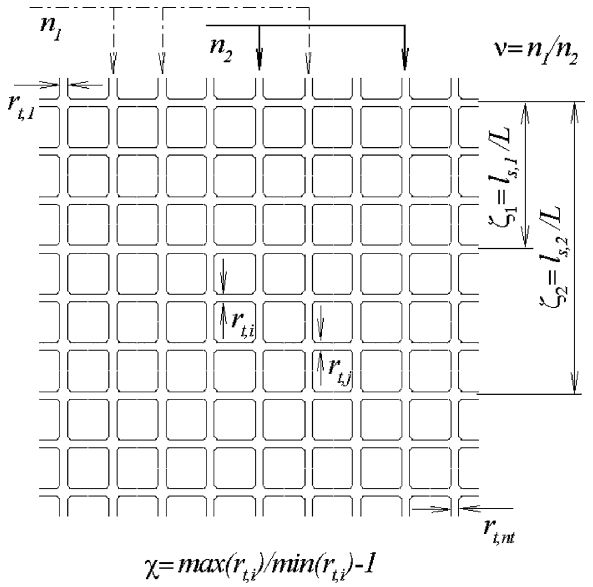

Fig. 1. Network model of a porous medium consisting of pores and throats. The flow parameters are shown: occurrence frequency of the phases at the network inlet ($\nu = n_1/n_2$), medium heterogeneity ($\chi = r_{max}/r_{min} - 1$), and the length scale representing the cluster size ($\zeta = l_s/L$).

medium and form distinct flow patterns. The irregularity of the pattern of each phase is caused by local heterogeneities that produce local variations of permeability (K) and capillary pressure (p_c), which in turn result in local flow rate variations for each phase. The heterogeneity is determined by the prescription of the throat radii (r_t) using a predefined distribution function. For a uniform distribution of throat radii (r_t) with a minimum (r_{min}) and maximum (r_{max}), $r_{min} < r_t < r_{max}$, the heterogeneity parameter can be defined as $\chi = r_{max}/r_{min} - 1$, and in the limit of a homogeneous sample we have $\chi = 0$. It should be noted that a pore network does not provide a direct geometric representation of a physical porous medium. Physical consistency is ensured by selecting a throat radii distribution function such that K and p_c in the numerical network are physically representative of values measured in the actual porous medium of interest.

Viscous forces influence the length scale for which the parts of one phase are fully surrounded by the other. The size of the entrapped phase (cluster) is a measure of the viscous correlation length. Still, the capillary force controls the phase displacement on the local level [32]. Therefore, a length scale (l_s) is defined that is smaller or equal to the domain length (L) in the network where the invasion of phases occurs (note that l_s differs from the correlation length). Once some fraction of the throats is invaded over a length l_s, the throats in the next layer of the network of length l_s are allowed to be filled. This is repeated until all layers of length l_s in the network are filled. Hence, for a length scale l_s which is equal to the length of the domain (L), the process is governed by capillary forces and corresponds to a small capillary number. As the length scale l_s decreases, the filling is increasingly controlled by viscous forces, which coincides with a larger capillary number. To vary the length scale l_s, the process extent parameter ($\zeta = l_s/L$) is defined and used (see Fig. 1).

Satisfying the condition that the spread of phases is governed by capillary forces at the local level, the invasion percolation with trapping algorithm [21] is used for both phases. Each phase occupies different throats in the network and there is no momentum transport between them. At the onset, the spread of both phases starts into a network completely filled by the first phase (originally present). This first phase, together with the other (second) phase,

enters the network. As two mobile phases are present, different types of clusters can be formed, and the trapping rules must be modified. The set of rules for how the phases are allowed to spread within the network are:

(i) for each of the two phases, the carrying backbone is defined as a flow path that spans the network inlet and outlet,
(ii) the paths of the different phases can intersect within the network,
(iii) only clusters of the originally present phase in the network can be formed, and they are surrounded by either of the two phases' preferential flow paths.

The clusters which are surrounded by the originally present (first) phase flow paths contribute to momentum transport (they are part of the carrying backbone of the originally present phase) and they are mobile. In this case, mobile means that the fluid phase is mobile, but the corresponding clusters stay in the same position. On the other hand, clusters of the first phase which are surrounded by flow paths of the other (second) phase do not contribute to momentum transport, and in these clusters, the first phase is immobile. Clusters of the second phase cannot form; however, there are still parts of the second phase that do not belong to the second phase backbone and do not contribute to momentum transport. Finally, throats that belong to the clusters which are formed by first phase flow paths (mobile clusters) can be invaded by the second phase.

Within the network, there are parts of each phase that belong to each phase carrying backbone (mobile) and parts that are immobile. Thus, the content of each phase is given as a phase saturation s_1 and $s_2 = 1 - s_1$, and the immobile parts are defined as immobile saturations $s_{im,1}$ and $s_{im,2}$. Since each throat is occupied by only one phase, the saturation is a ratio of the volume of throats filled with a particular phase ($V_{t,i}$) to the volume of all throats ($V_{t,all}$):

$$s_i = \frac{\sum_j V_{t,i}^j}{V_{t,all}}, \tag{1}$$

where the index i refers to the phases ($i = 1, 2$), and the index j is a summation index. Similarly, the immobile saturation can be obtained by adding the volumes of throats filled by immobile phase.

In single-phase flow, the network as depicted in Fig. 1 shows the flow resistance, which is defined as a single phase permeability (K_{sp}) or network permeability, and is calculated from Darcy's law. This permeability is a function of porosity, $K_{sp} = K_{sp}(\phi)$. With two phases present, the flow resistance of each phase becomes larger compared to single-phase flow. For multiphase flow, it is assumed again that the phase velocity ($\mathbf{u}_i$) and the phase pressure gradient (∇p_i) are related linearly according to Darcy's law. The proportionality constant is phase specific and depends on the phase permeability (K_i) and the phase viscosity (μ_i) ($i = 1$ or 2). Thus, for each phase [33]:

$$\mathbf{u}_i = -\frac{K_i}{\mu_i}\nabla p_i, \tag{2}$$

where the phase permeability (K_i) is a function of porosity (ϕ) and saturation (s), $K_i = K_i(\phi, s)$. In order to separate the influence of the saturation, the relative permeability ($k_{r,i}$) of each phase ($i = 1, 2$) is defined as a ratio of the phase permeability to the single phase permeability:

$$k_{r,i} = \frac{K_i}{K_{sp}} = \frac{Q_i}{Q}. \tag{3}$$

As shown in the above relation, given an applied pressure drop in the network ($\Delta p/L$), the relative permeability can be obtained as a ratio of the phase flow rate (Q_i) to the single-phase flow rate through the network (Q).

At the interface between two phases, a potential difference across the interface can be defined. In order for one phase to spread into another, it is not sufficient to have a potential difference at the interface, but the difference must also be larger than the threshold potential. Furthermore, due to heterogeneities of the local medium, the threshold potential varies both along the interface, as well as with the motion of the interface during the invasion. In the network, the potential difference is given by the pressure difference between two connected pores. The threshold potential difference is the capillary pressure of the connecting throat (p_c), calculated from the Young–Laplace equation:

$$p_c = \frac{2\sigma}{r_t}, \tag{4}$$

where σ is the surface tension of the originally present phase, and r_t is the radius of the throat. This displacement criterion requires the solution of the pressure field during invasion. However, in the limit of very slow processes (capillary force dominated) this criterion turns into a simpler rule: in a drainage-like process, the throat with the largest radius will be invaded. For faster flows (viscous force dominated) the same rule (largest throat radius) for the spread of phases can be exploited, but the maximum cluster size decreases as the phase velocity increases (the cluster size is limited using l_s).

3. Numerical procedure

A two-dimensional, regular square network of size ($n_L \times n_L$) is defined using throats with circular cross-sections and four throats connected to each pore. Two phases, one of which is the same as the initial phase, enter the network at the inlet boundary. The outlet is on the opposite side of the network. There is no flow across the remaining two network boundaries. Phases enter the network alternately, and the number of consecutive steps of each phase is n_1 and n_2, respectively. If one phase is dominant, it might block the other phase, preventing it from reaching the network outlet. In this case, a deficient phase becomes a large stationary cluster in the network.

Once there are no available throats to be filled, the pressure for each phase within the network is calculated. It is assumed here that the phases are in equilibrium. Thus, there is no transport across the interface (the interface is stationary), and each phase flows only from the network inlet to the outlet. Only the phase carrying backbone contributes to the momentum transport and to the phase relative permeability. If one phase does not reach the outlet, this phase is regarded as a cluster, and a solution of the pressure is not required. For the phase(s) flowing through the network, the pressure solution is found by applying a mass balance at each pore within the network. The balance for one pore (i) is given in the form of the flow rates through all connected throats ($q_{i,j}$) and has the form:

$$\sum_{j=1}^{c} q_{i,j} = 0, \quad c = 4, \tag{5}$$

where c is the flow coordination number. In single-phase flow, the flow and network coordination numbers are equal. However, in multiphase flow, the flow coordination number is defined for pores that belong to the phase carrying backbone. In general, c varies throughout the backbone, where for any pore, one or more throats can be occupied with another phase. The flow rate ($q_{i,j}$) through each throat ($j = 1, \ldots, c$) is calculated from its conductance (g_j) and the pressure difference (Δp) at the starting and ending pore of the throat as:

$$q_{i,j} = g_j \Delta p. \tag{6}$$

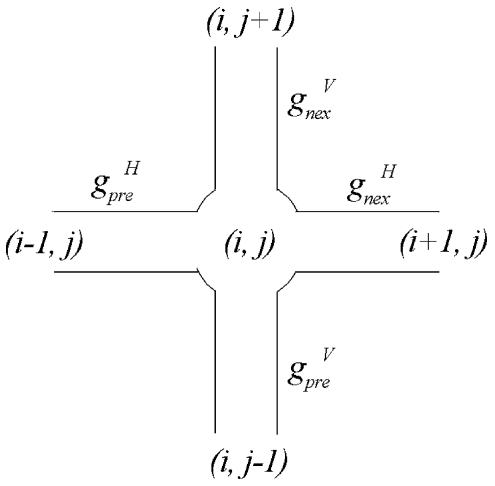

Fig. 2. Network node with one pore and connecting throats.

For a circular throat of radius ($r_{t,j}$) and length (l_t), the exact value of the conductance is obtained from the Poiseuille solution:

$$q_j = \frac{\pi r_{t,j}^4}{(8\mu l_t)}, \tag{7}$$

where μ is the viscosity of the phase for which the pressure solution is solved ($\mu_1 \neq \mu_2$).

Applying the balance equation to each pore, Eq. (5) can be assembled over the whole network (single phase flow) or phase carrying backbone. Fig. 2 shows a pore (i, j) and four connecting throats: ($i-1$, j), ($i+1$, j), (i, $j-1$) and (i, $j+1$). Both horizontal (H) and vertical (V) throats can be *previous* (*pre*) or *next* (*nex*) to the pore (i, j). Since the direction of the flow for each throat is not known *a priori*, all (q_j) are defined as the flow into pore (i, j). Using this convention and Eq. (5), the mass balance for pore (i, j), obeys:

$$g_{pre}^{H}p_{-10} + g_{nex}^{H}p_{+10} + q_{pre}^{H}p_{-01} + g_{nex}^{V}p_{+01} - (g_{pre}^{H} + g_{nex}^{H} + q_{pre}^{H} + g_{nex}^{V})p_{00} = 0, \tag{8}$$

where the subscripts for pressure (p) and conductance (g) are in reference to Fig. 2. In multiphase flow, the throats that do not belong to the carrying backbone of the current phase are omitted, as they do not contribute to the balance of the current phase. Applying Eq. (8) to each pore yields a linear system of algebraic equations for the pressure ($\mathbf{p}$) over the network/carrying backbone. Hence, one can write:

$$\mathbf{A}_i\mathbf{p}_i = \mathbf{b}_i, \tag{9}$$

with index i referring to the single phase ($i = sp$) or multiphase flow (phases, $i = 1, 2$). The matrix ($\mathbf{A}_i$) is obtained from the conductances of throats, whereas the force vector ($\mathbf{b}_i$) depends on both throat conductances and the external pressure at the inlet and outlet of the network.

Eq. (9) is solved once for single-phase flow over the whole network and twice for the two phases over corresponding carrying backbones. Having determined the pressure distribution, the flow rate is calculated by summing the flow rates through the throats at the inlet or the outlet boundary. Once an equilibrium distribution of phases in the network is achieved, mass conservation requires that the flow rate of each phase into the network equals the flow rate out of the network. For phase i, the flow rate at the inlet is:

$$Q_i^{inlet} = \sum_m g_m(p_{inl} - p_m), \tag{10}$$

where m is a summation index for all throats occupied by phase i. From the single-phase flow rate (Q_{sp}), the network or single-phase permeability (K_{sp}) can be computed from Darcy's law. Similarly, both phase permeabilities (K_i) are obtained from known phase flow rates (Q_i). The relative permeabilities are then calculated from Eq. (3). The flow through the network is two-dimensional, whereas all permeabilities are calculated for, in-principle, one-dimensional flow. Therefore, for a fluid of viscosity (μ):

$$K = \mu\frac{Q}{A}\frac{L}{\Delta p}, \tag{11}$$

where K and Q are used for either single phase (sp) or multiphase flow (i). The pressure drop in the network is $(p_{in} - p_{out})/L$ and $u = Q/A$ is the superficial velocity. Finally, the capillary pressure (p_c) is found by averaging the local capillary pressures (Eq. (3)) over the entire static interface in the spread termination point.

4. Results and discussion

The numerical results are obtained for a regular square network ($n_L \times n_L$) of size $n_L = 60$. The cylindrical throats have dimensions (r_t, l_t), where the throat length $l_t = 2 \times 10^{-4}$ m. The heterogeneity parameter (χ), the occurrence frequency ($\nu = n_1/n_2$), and the process extent ($\zeta = l_s/L$) are altered in order to vary the regimes and obtain a broad range of phase distributions within the network. Local heterogeneities are included by setting the throat radius as a random variable. In this study, the radii are uniformly distributed in the range (r_{min}, r_{max}) with an average radius $r_{av} = 4 \times 10^{-4}$ m. The minimum (r_{min}) and maximum (r_{max}) radii are set to $(r_{min}, r_{max}) \times 10^{-4}$ m = {(3.5, 4.5), (2.0, 6.0), (0.5, 7.5)}, with a corresponding heterogeneity parameter ($\chi = r_{max}/r_{min} - 1$) equal to $\chi = \{0.3, 2, 14\}$ ranging from almost homogeneous to highly heterogeneous media. Either phase – water or air – can be in excess or deficient compared to the other phase, and therefore, seven distinct values of ν are used, $\nu = \{0.1, 0.25, 0.5, 1, 2, 4, 10\}$. The maximum distance ($l_s$) between two throats that are filled successively is initially set equal to the network length (L) which corresponds to capillary force controlled regime. This distance is gradually decreased to $l_s/L = 1/20$ for fast water transport corresponding to the viscous force controlled regime; thus $\zeta = \{1, 1/3, 1/10, 1/20\}$. Overall ($\nu$, χ, ζ) = $(7 \times 3 \times 4) = 84$ different combinations of parameters are investigated. Finally, for each combination (ν, χ, ζ), the throat radii (r_t) are randomly generated $N = 20$ times, and the results of all realizations are used to obtain statistical averages.

Once the distribution of the phases is obtained, the saturation is calculated from Eq. (1) by summing the volumes of throats occupied by each phase. Similarly, the immobile saturation of each phase is found, but only for the throats in which flow rate is equal to zero. The capillary pressure is calculated at the phase interfaces. As the spread of both phases is locally governed by capillary forces, p_c is found by averaging the capillary condition (Eq. (4)) at the interfaces. The single-phase, and the phase permeabilities are found from the phase flow rates across the boundary (Eq. (10)) and Darcy's law (Eq. (11)).

4.1. Initial analysis

A typical solution containing the distribution of the two phases is shown in Fig. 3(a); the originally present phase (first phase) is shown with gray lines, whereas the second phase is depicted by black lines. The carrying backbones of both phases are shown in Fig. 3(b). In this case, the numbers of invading steps are equal ($n_1 = 1$ and $n_2 = 1$) and occurrence frequency, ν is equal to one. The length scale (l_s) is equal to the length of domain (L), and $\zeta = l_s/L = 1$. As invasion percolation with trapping is used for the distribution of phases, the heterogeneity parameter (χ) does not influence the spread of phases. The next throat to be invaded has to be the largest among all available throats. As can be observed from Fig. 3, the distribu-

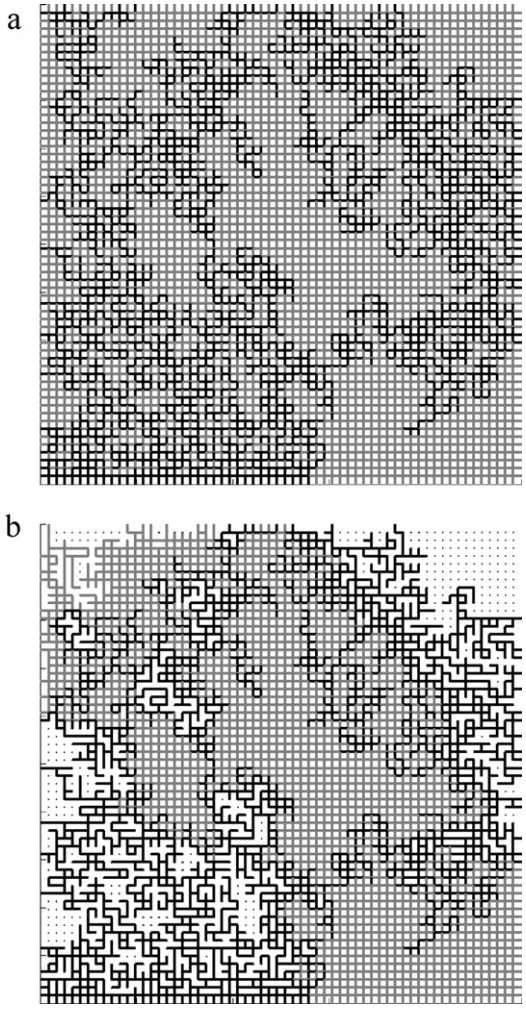

Fig. 3. Two mobile phases invasion of a capillary network: (a) distribution of phases in the termination point; (b) phase carrying backbones. The originally present (first) phase and the second phase are represented by gray and black lines, respectively. The inlet is at the top of network.

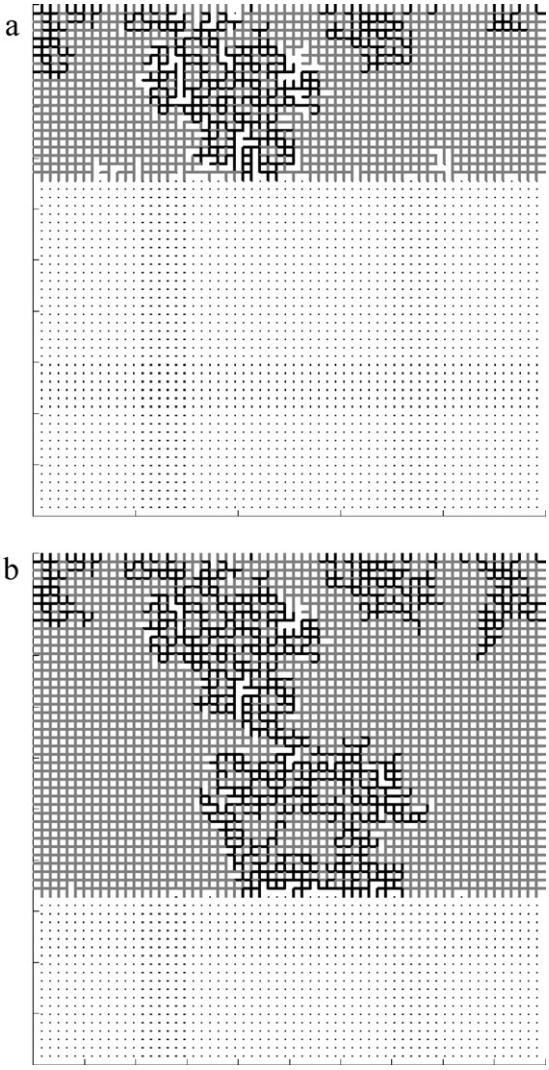

Fig. 4. The invasion percolation with defined cluster size and trapping for the maximum cluster size equal to one third of the network size: (a) after filling of first third; (b) after filling of second third.

tion of the two phases is asymmetric. Although $\nu = 1$ and one would expect equal saturations of each phase ($s_1 = s_2 = 0.5$), the saturation of the originally present phase is larger (in this realization $s_1 \approx 0.55$ and $s_2 \approx 0.45$). This difference is caused by the formation of clusters, as the second phase cannot spread into the immobile clusters of the first phase and one obtains $s_1 > \nu/(\nu+1)$ and $s_2 < 1/(\nu+1)$. The throats associated with the immobile first phase consist of: (a) throats surrounded by the flow path of the second phase, and (b) paths of the first phase that are not part of the carrying backbone. On the other hand, the throats associated with the immobile second phase belong to the second phase paths only, but not to the second phase carrying backbones; hence $s_{im,1} > s_{im,2}$. This is related to the momentum transport associated with the first phase (mobile) clusters. These are formed as parts of the first phase, which are surrounded by preferential flow paths of the same phase (see Fig. 3(b)). The mobile regions have low flow resistances which cause two relative permeabilities to differ ($k_{r,1} > k_{r,2}$).

Once the capillary number increases, the fluid spread is more localized and only throats which are within a distance of l_s may be filled in two consecutive steps. This stabilizes the fluid front and the flow becomes dominated by viscous forces. As a result of flow stabilization, smaller clusters are formed. Fig. 4 shows the filling of the network for $\zeta = l_s/L = 1/3$ after the first (Fig. 4(a)), and the second (Fig. 4(b)) layer of the network is filled. However, changes in l_s do not only alter the cluster size, but also cause segregation of the phases. This segregation allows two processes to occur: (i) channeling of phases and (ii) no-percolation of the deficient phase. The first process is promoted by decreasing l_s and the latter one is observed for large values of l_s. In order to quantify the percolation of the phase, the dimensionless fluid front position is defined as a ratio of the furthest fluid point from the inlet (l_{front}) to the length of the network (L):

$$\lambda_i = \frac{l_{front}}{L}. \tag{12}$$

Thus, the phase percolation occurs once $\lambda_i = 1$, and the condition of no-percolation corresponds to $\lambda_i < 1$. It can readily be seen that for the phase that does not percolate, the phase saturation (s_i) is equal to the immobile phase saturation ($s_{im,i}$), and the relative phase permeability is equal to zero.

In an ideal case, for multiphase parallel flow in which clusters do not form, saturation is proportional to the occurrence frequency ($\nu = n_1/n_2$), and can be expressed as $s_1 = \nu/(\nu+1)$ and $s_2 = 1/(\nu+1)$. This condition is satisfied for very low (ζ), which corresponds to the flow dominated by viscous forces. Otherwise, as ζ increases, the influence of capillarity becomes significant, and we obtain $s_1 > \nu/(\nu+1)$ and $s_2 < 1/(\nu+1)$. This is shown in Fig. 5(a), where the

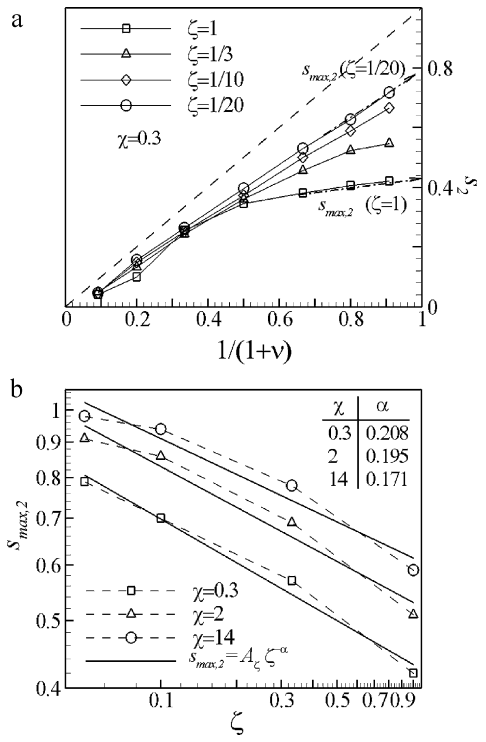

Fig. 5. Estimation of the second phase maximum saturation ($s_{max,2}$) for different heterogeneity and process extent (χ, ζ): (a) extrapolation for $\chi = 0.3$ and all ζ investigated with dash line limit $s_2 = 1/(1+\nu)$, and (b) power law dependence of $s_{max,2}$ as a function of the cluster size.

plots s_2 *vs.* $1/(1+\nu)$ for constant heterogeneity $\chi = 2$, and for various $\zeta = l_s/L$ are depicted. The dashed line represents $s_2 = 1/(1+\nu)$, and it can be observed that the actual value of s_2 is lower than the limiting value $1/(1+\nu)$. However, as the heterogeneity increases, s_2 approaches $1/(1+\nu)$ as the throats that are filled are larger and contribute the most to the medium volume. The second phase saturation is extrapolated as ν tends to zero and $1/(1+\nu)$ goes to the intrinsic saturation value. This saturation is referred to as the maximum achievable saturation ($s_{max,2}$) of the second phase; $s_{max,2}$ depends on ζ and χ, and the results are depicted in Fig. 5(b). In Fig. 5(b), the symbols represent the numerical results, and the solid lines represent the power law fits:

$$s_{\max,2} = A_\zeta \zeta^{-\alpha}. \tag{13}$$

The results yield exponents in the range $\alpha \approx 0.17$–0.2, with α decreasing with χ. The existence of the maximum saturation of the second phase ($s_{max,2}$) suggests that there is an additional property of two-phase flow: the content of the originally present phase that cannot be displaced from the network even when the second phase is dominant (in this case ν is very small). This retention of the first phase is caused by its immobile clusters, around which the second phase flows. The amount of the phase that cannot be displaced can be quantified as an irreducible saturation ($s_{ir,1}$) of the first phase. The value of $s_{ir,1}$ is related to $s_{max,2}$, and the irreducible saturation of the originally present phase (first phase) is:

$$s_{ir,1} = 1 - s_{\max,2}, \tag{14}$$

where $s_{max,2}$ is estimated from the dependence s_2 and ν as shown in Fig. 5(a).

4.2. Single ($k_{r,i}$–s–p_c) and (λ_i–s) curves

In order to assess how the relative permeabilities ($k_{r,i}$), capillary pressure (p_c), and fluid fronts (λ_i) of each phase change as a function of saturation (s_i), simulations were performed with constant values for χ and ζ, and by varying $\nu = n_1/n_2$. For each value of ν, the distribution of throat radii (r_t) is generated randomly ($N = 20$) to obtain stochastic averages. Hence, 140 discrete points (ν, N) = (7×20) were used to generate ($k_{r,i}$–s_i–p_c) and (λ_i–s_i) curves. The relative permeability $k_{r,1}$ is equal to the permeability ratio K_1/K_{sp}, where the phase permeability (K_1) is found using the generalized Darcy's law (Eq. (11)) from the known pressure drop, and calculating the phase flow rate at the network flow boundary (inlet or outlet, Eq. (10)). The second phase relative permeability ($k_{r,2}$) is determined in the same manner. The saturation of the originally present phase (first phase, s_1), and the immobile saturations ($s_{im,1}$) and ($s_{im,2}$) are computed from the whole network. The capillary pressure is averaged at the interface between the second phase carrying backbone and the remaining part of the network. The results for $k_{r,1}$, p_c, and λ_1 for $\zeta = 1$ and $\chi = 14$ are shown in Fig. 6(a)–(c). The circles represent the discrete realizations, and the bold squares show the averages for each value of ν. The standard deviations are also shown (error bars) in the figure, with the horizontal error bars representing the saturation deviation. It can be seen from Fig. 6(a) that for some random network corresponding to a small value of ν (the second phase is dominant), the relative permeability $k_{r,1}$ is equal to zero (*i.e.* there is no percolation of the first phase). As ν increases, the first phase percolates, and s_1 and $k_{r,1}$ increase. Therefore, as long as $k_{r,1} = 0$, the fluid front (λ_1) is less than one. The effect of s_1 on the fluid front is shown in Fig. 6(c). As s_1 increases, the first phase protrudes more into the network and λ_1 increases and eventually becomes equal to one. Remarkably, Fig. 6(b) exhibits a relatively constant capillary pressure irrespective of saturation. This implies that for specified values of χ and ζ, the distribution of throat sizes at the interface remains constant regardless of changes of the flow patterns and interface shapes with s_1.

A power law is usually used to correlate the relative permeability ($k_{r,i}$) and the saturation (s_i) in a form $k_{r,i} = Bs_i^{\beta}$. Such a comparison for a heterogeneity ($\chi = 14$) and all four investigated ζ is given in Fig. 7(a) and (b). In Fig. 7, the symbols represent averaged numerical results, and the solid $\zeta = 1/20$ and dash-dot $\zeta = 1$ lines are the lower and upper power law approximations. For the originally present phase (first phase), the value of the exponent (β) decreases from $\beta = 2.8$ to $\beta = 1.7$ as ζ decreases from $\zeta = 1$ to $\zeta = 1/20$ (this corresponds to an increase of the capillary number). Similarly, for the second phase, the power decreases from $\beta = 1.4$ to $\beta = 1.3$ with decreasing ζ. On the other hand, β is much less sensitive to variations in χ, and remains almost constant for distinct χ (a change in β around 0.1–0.2 for both permeabilities – results are not shown here). Furthermore, the parameter (B), which accounts for the irreducible saturation of the first phase, approaches unity as ζ decreases. From the fact that $k_{r,i} = 0$ for a phase (i) which does not percolate, $k_{r,i}$ should be correlated as a function of $(s_i - s_{im,i})$ in order to obtain $k_{r,i}(s_i - s_{im,i} = 0) = 0$. Hence, the following relationship is used:

$$k_{r,i} = B_k(s_i - s_{im,i})^{\beta_k}, \tag{15}$$

where B_k and β_k are again parameters to be estimated, and where they are influenced by χ and ζ. The shift in the ($k_{r,i}$–s_i) curves from Fig. 7 to account for $s_{im,i}$ is shown in Fig. 8 (symbols – numerical results, and lines – power law). The values of the exponent (β_k) decrease compared to β and range from 1.3 to 1.8 for the first phase, while remaining essentially constant for the second phase $\beta_k \approx 1.2$. The relative permeability does not, however, follow the power law over the entire range of saturation differences

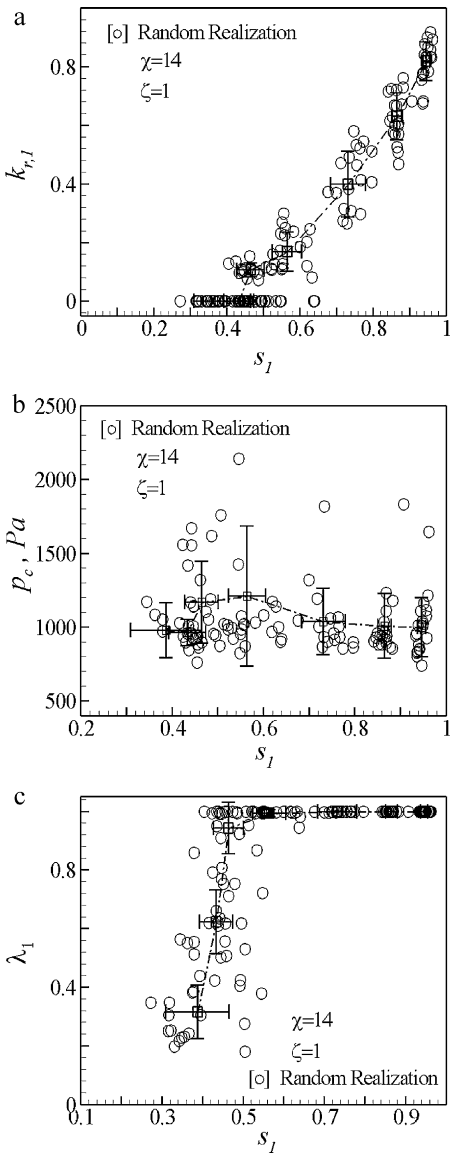

Fig. 6. Possible values of (a) first phase relative permeability ($k_{r,1}$), (b) capillary pressure (p_c), and (c) first phase fluid front (λ_1) for network random realizations over entire range of saturations. These are given with open circles; averages are shown with bold squares and corresponding standard deviations with error bars (horizontal for saturation).

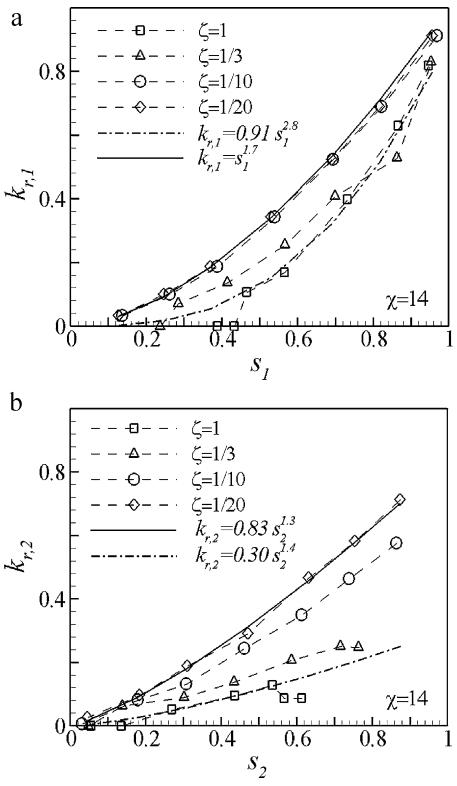

Fig. 7. Relative permeability as a function of phase saturation for different cluster size (symbols): (a) first phase; (b) second phase. The lower and upper power law limits are plotted with dash-dot and solid lines, respectively.

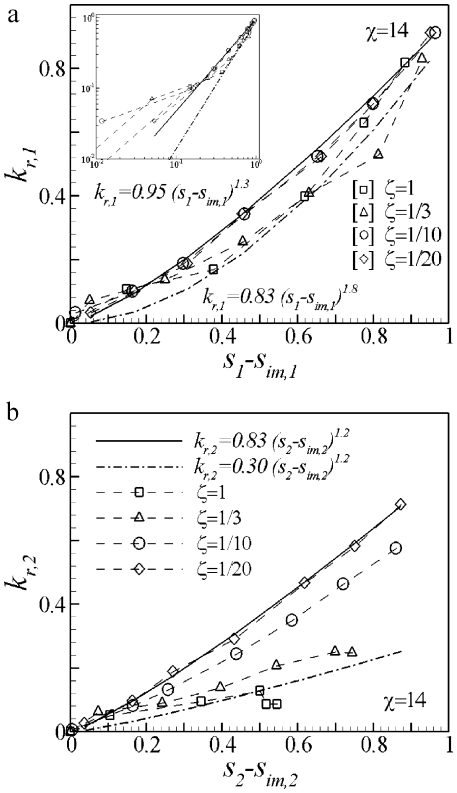

Fig. 8. Relative permeability as a function of phase saturation shifted for a phase immobile saturation, and lower (dash-dot) and upper (solid line) power law approximation: (a) first phase; (b) second phase. Distinct cluster sizes (ζ) are represented by different symbols.

($s_i - s_{im,i}$), as can be seen from the inset *log–log* plot in Fig. 8(a). For small saturation differences, $k_{r,1}$ deviates from the power law estimated for higher saturation differences. As for B, the values of B_k are close to one in all cases, except for the second phase and $\zeta \approx 1$, suggesting again that for unstable flows the originally present phase (the first phase), cannot be completely displaced, and hence $s_{ir,1} > 0$.

4.3. Influence of χ and ζ

In order to determine how the ($k_{r,i}$–s–p_c) and (λ_i–s) curves change with heterogeneity (χ) and the cluster size length scale (l_s) (process extent, $\zeta = l_s/L$), the numerical results for all investigated pairs (χ, ζ) are averaged (as shown in Figs. 6(a)–(c) for $\chi = 2$ and $\zeta = 1$). The relative permeability ($k_{r,i}$) is a phase permeability (K_i) ($i = 1, 2$) normalized with respect to the single-phase permeability (K_{sp}). Both K_i and K_{sp} are influenced by χ. The single-phase perme-

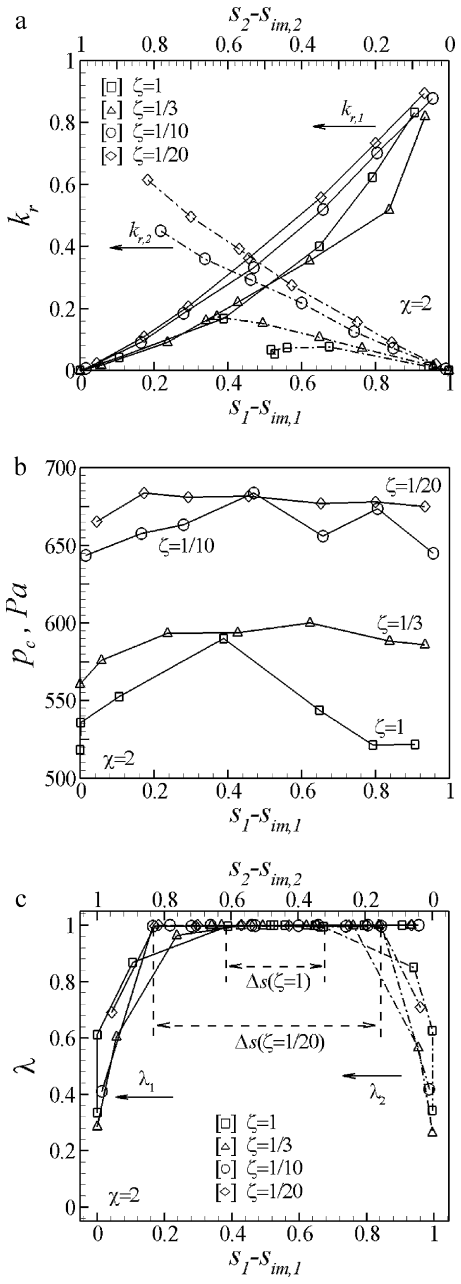

Fig. 9. Influence of cluster size (ζ) on (a) relative permeabilities, (b) capillary pressure, and (c) fluid fronts. In part (c), the saturation range for which both phases percolate is given with Δs.

ability decreases as the medium heterogeneity increases, whereas for a drainage like process, where the largest throats are occupied, K_i increases with χ. There is no influence of ζ on K_{sp}, but K_i depends on ζ and thus, so does $k_{r,i}$. Conversely, the capillary pressure should be a strong function of the porous medium heterogeneity (Eq. (4)) and of the process extent. Both parameters change the throat size distribution at the interface. For larger χ, the influence of small throats is larger and p_c increases; for larger ζ, the phases are less segregated and the throat radii at the interface are shifted toward larger values, and hence, to smaller p_c. The fluid fronts and no-percolation regime are strongly influenced by ζ and to a lesser degree by χ.

Fig. 9 shows how all five parameters change with saturation and ζ for constant $\chi = 2$. The originally present phase (first phase) and the second phase are depicted by solid and dash-dot lines, respectively. Different symbols are used for distinct values of ζ. When $k_{r,i} = 0$ for phase (i), there is no percolation, the immobile part of the phase does not contribute to the momentum transport, and the relative permeabilities are given as a function of $(s_i - s_{im,i})$ (Fig. 9(a)). As can be observed from Fig. 9(a), there are large differences between the two relative permeabilities $k_{r,1}$ and $k_{r,2}$ as function of the cluster size (l_s) (parameter ζ). Both relative permeabilities increase as ζ decreases, because the flow stabilization causes the clusters to become smaller. Hence, a larger part of the porous medium is available to the flow, resulting in an increases in $k_{r,i}$. This increase is more prominent for the second phase, whereas regardless of ζ, $k_{r,1}$ increases only slightly (the mobile clusters of the first phase are always present). The two permeabilities, $k_{r,1}$ and $k_{r,2}$ are not symmetric, with $k_{r,2}$ having maximum values smaller than one. This is due to the fact that the second phase mobile clusters do not exist, and the second phase meanders throughout the network around large clusters of the first phase (mobile or immobile). However, as ζ decreases and the phases segregate, both phases behave like the single phase, and the relative permeability is influenced by the porous medium volume occupied by that phase. Both relative permeabilities become more symmetric, and change almost linearly with s_i.

The changes of the capillary pressure (p_c) with ζ are largely influenced by the heterogeneity parameter (χ). Thus, for a network that is close to homogeneous (all throats have similar sizes), the capillary pressure is constant with ζ. For a heterogeneous network, as the preferably filled throats and the interface shape change with ζ, a variation in p_c is observed as shown in Fig. 9(b) for four different values of ζ. The capillary pressure increases as ζ decreases, where the throats with smaller radii become part of the interface for smaller ζ. Furthermore, and as observed earlier, the capillary pressure (p_c) does not change with saturation when ζ is held constant. In the latter case, the only change that occurs with varying saturation (s) is the interface shape, but the average radius of the interfacial throats remains constant. For small ζ, the effects of phase channeling are observed. Both phases percolate, and the fluid front positions are $\lambda_i = 1$. As ζ increases, the fluid flow becomes unstable and one phase can be blocked by the other. The deficient phase therefore does not reach the outlet, $\lambda_i < 1$. Fig. 9(c) shows the fluid front positions (λ_i) where, for distinct ζ, different saturation widths (Δs) are obtained for which both phases percolate. In general, Δs increases as ζ decreases.

It is instructive to examine how the porous medium heterogeneities (χ) influence ($k_{r,i}$–s–p_c) and (λ_i–s) curves, and these results are shown in Fig. 10(a)–(c) (for $k_{r,i}$, p_c, and λ_i, respectively). Again, as in Fig. 9, the first phase is plotted with solid lines, and the second phase with dash-dot lines. Different symbols are used for three values of χ, with the length scale held constant $\zeta = 1$. The capillary pressure is a strong function of χ. On the other hand, a comparison between $k_{r,1}$ and $k_{r,2}$ reveals that $k_{r,1}$ is a weaker function of χ, whereas $k_{r,2}$ increases twofold as χ changes from $\chi = 0.3$ to $\chi = 14$. For the first phase, this fact might be attributed to the mobile clusters of the first phase (originally present phase), where the clusters are sufficiently large that they represent the momentum transport hindrance caused by heterogeneities (χ) in the same manner as the overall network. Thus, one does not observe changes of $k_{r,1}$ with χ; this is corroborated with percolation results for the fluid front (λ_1) (solid lines in Fig. 10(c)). No noticeable changes of λ_1 with s_1 for different χ are observed, and the first phase volume follows the increase of the volume of the overall network. Therefore $s_2 = 1 - s_1$ is also not influenced by χ, and the increase in $k_{r,2}$ may be purely caused by the larger radii of the second phase flow paths with increasing χ. The influence of χ on the capillary pressure is more pronounced than on $k_{r,i}$ and λ_i. As χ increases, some parts of the interface will have smaller throat radii with larger capillary pressures. Finally, p_c does not depend on saturation for a given

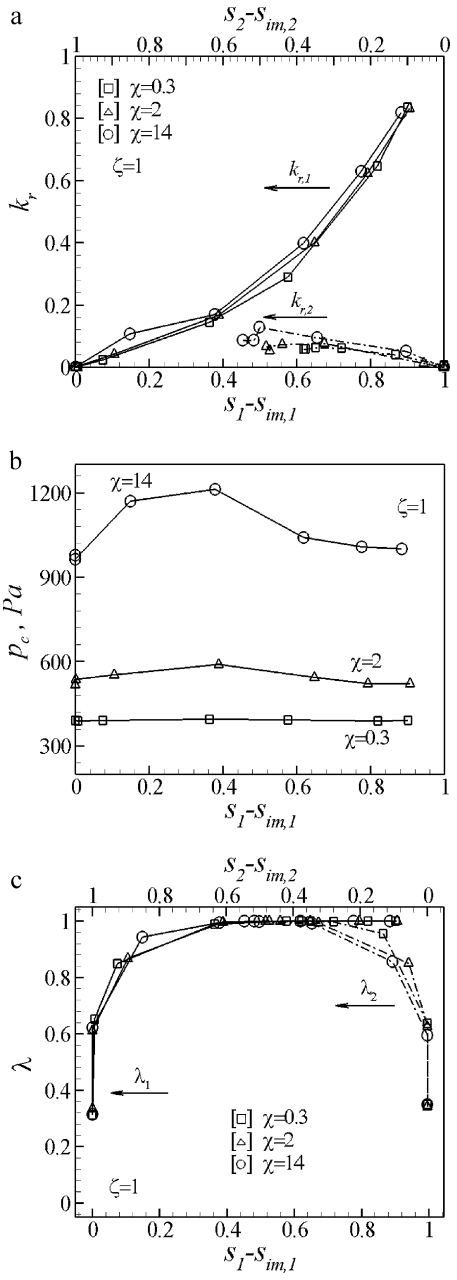

Fig. 10. Variation of (a) relative permeability, (b) capillary pressure, and (c) fluid fronts with medium heterogeneity (χ) for large clusters, $\zeta = 1$. The second phase relative permeability, $k_{r,2}$ is for an order of magnitude lower than $k_{r,1}$ due to the mobile clusters of the first phase.

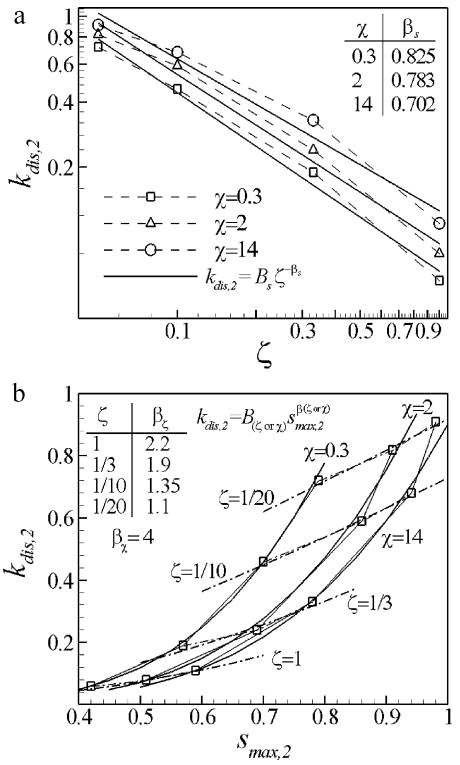

Fig. 11. Displacement flow relative permeability ($k_{dis,2}$): (a) variation with χ and ζ and power law approximations; (b) envelope ($k_{dis,2}$–$s_{max,2}$) and the saturation power laws. The saturation power laws differ from one obtained for two mobile phases flow.

χ, as interface radii average to the same values regardless of the saturation.

4.3.1. Displacement flow

In the limit when $\nu = n_1/n_2$ becomes small (the second phase is dominant) and approaches zero, the parallel flow becomes a displacement flow. Here, the second phase is mobile, whereas the originally present phase (first phase) is distributed in the network as immobile clusters. For this case, the second and first phase saturations are referred to as the maximum saturation ($s_{max,2}$) and irreducible saturation ($s_{ir,1}$), respectively. The saturation $s_{max,2}$ is found by extrapolating data from Fig. 5(a). Similarly, the relative permeability of the displacement flow ($k_{dis,2}$) is obtained by extrapolating from the ($k_{r,2} \sim s_2$) dependence in the limit of s_2 approaching unity. Thus, $k_{dis,2}$ becomes an intrinsic value of $k_{r,2}$. The permeability $k_{dis,2}$ is a function of both χ and ζ, where it is assumed $k_{dis,2} = B_s \zeta^{-\beta_s}$ and B_s and β_s are parameters that depend on χ. The results of such a comparison are shown in Fig. 11(a) with extrapolated $k_{dis,2}$ given by the symbols connected with dashed lines, and the power law approximation is shown with solid lines. Both $s_{max,2}$ and the permeability $k_{dis,2}$ increase with χ. Here, B_s and β_s depend on χ, and β_s decreases as χ increases. The parameter β_s is found to be in the range of 0.7–0.8.

The saturation ($s_{max,2}$) can be interpreted as an equilibrium saturation of the displacing phase. This saturation depends on χ and ζ (Fig. 5(b)), and in order to obtain ($k_{dis,2}$–$s_{max,2}$) curves, the saturation results shown in Fig. 5(a) are correlated with the permeability data in Fig. 11(a). The results are presented in Fig. 11(b), where the numerical points ($s_{max,2}$, $k_{dis,2}$) are depicted with square symbols, and power law fits are shown with solid lines for constant χ with power β_χ, and dash-dot lines for constant ζ with power β_ζ. In displacement flow, β_ζ is found to vary in the range of 1.1–2.2, whereas the influence of the cluster size ζ on the power β_χ is much higher, and $\beta_\chi = 4$ for all χ. The values of the exponents imply that ζ has a larger influence than χ on the relative permeability; the same trend was observed in the flow of two mobile phases. It should be noted here that the exponents β and β_k (see Eq. (15)), estimated for the second phase for flow of two mobile phases and constant χ, correspond to the power β_χ. However, β_χ is larger than β or β_k, suggesting that different mechanisms influence the displacement and flow of two mobile phases. The same relative permeability dependence cannot be used in both types of flow. This distinction does not apply to the capillary pressure, as p_c does not change with saturation in the flow of two mobile phases. The envelope for p_c is therefore a function of χ and ζ as shown in Fig. 12, but not of the flow type.

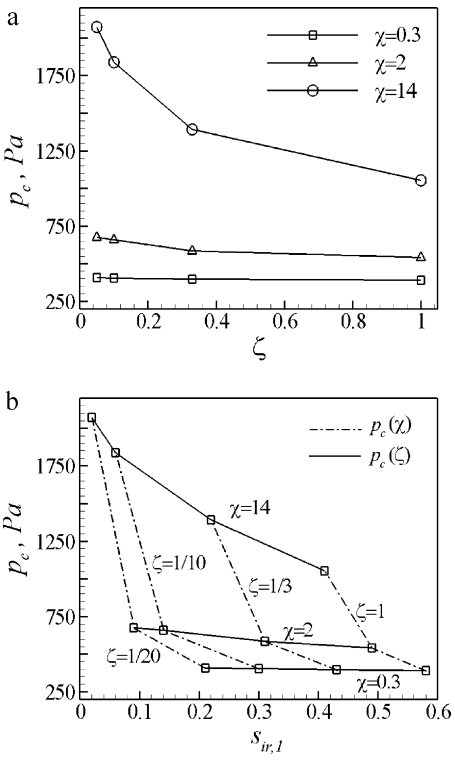

Fig. 12. Changes of the capillary pressure (a) as a function of medium heterogeneity (χ) and cluster size (ζ), and (b) construction of (p_c–$s_{ir,1}$) envelope for displacement flows, where $s_{ir,1}$ is irreducible saturation of the originally present phase. The envelope remains the same in two mobile phases flow as p_c is constant with s_1 (see *e.g.* Figs. 9(b) and 10(b)).

5. Conclusions

Two-phase flow, in which both phases are mobile and flow co-currently, has been investigated using an extended discrete pore network methodology. Functional changes in relative permeabilities, capillary pressure, and fluid fronts, as a function of phase saturation, have been predicted for conditions corresponding to a PEMFC gas diffusion layer. Two additional parameters have also been varied: the network heterogeneity and the process extent, which is a measure of the maximum allowed cluster size. It was found that the relative permeabilities follow a power law of saturation, with the permeability of the originally present phase exhibiting a higher sensitivity to saturation changes than the other phase. When the immobile phase saturation is accounted for by expressing the results in terms of the reduced phase saturation, smaller exponents are obtained. The numerical results suggest that the cluster size influences the exponent much more than the heterogeneity of the porous medium. For a defined porous medium and maximum cluster size, the capillary pressure does not change with the saturation, but it is found to vary significantly with the heterogeneity of the medium and the cluster size. For conditions that favor small throats at the interface, the capillary pressure increases. This is true for highly heterogeneous media and small clusters. The cluster size influences the percolation of the phases, and for small clusters the phase channeling occurs. For smaller clusters, range of phase saturations for which both phases percolate becomes broader.

Displacement flow is a limiting case of parallel flow, where the originally present phase in the network is highly deficient at the network inlet. Since the numerical simulations cover a wide range of saturations, parallel flow data was extrapolated for the originally present phase deficient at the inlet (second phase dominant). Relative permeability and capillary pressure curves were deduced from the extrapolation. The relative permeability is specific to the flow type and needs to be determined for each flow type (parallel or displacement). In displacement flow, relative permeability also follows a power law relationship, but the exponents are much higher than for parallel flow. The capillary curves, on the other hand, do not depend on the flow type.

References

[1] A.G. Yiotis, A.K. Stubos, A.G. Boudouvis, Y.C. Yortsos, Adv. Water Resour. 24 (2001) 439–460.
[2] J.H. Nam, K.J. Lee, G.S. Hwang, C.J. Kim, M. Kaviany, Int. J. Heat Mass Transfer 52 (2009) 2779–2791.
[3] N.C. Reis Jr., R.F. Griffiths, M.D. Mantle, L.F. Gladden, Int. J. Heat Mass Transfer 46 (2003) 1279–1292.
[4] T. Berning, N. Djilali, J. Electrochem. Soc. 150 (2003) A1589–A1598.
[5] N. Djilali, Energy 32 (2007) 269–280.
[6] M.C. Leverett, AIME Trans. 142 (1941) 152–169.
[7] K.S. Udell, Int. J. Heat Mass Transfer 28 (1985) 485–495.
[8] R.H. Brooks, A.T. Corey, Hydrol. Papers 3 (1964) 1–27.
[9] M.T. van Genuchten, Soil Sci. Soc. Am. J. 44 (1980) 892–898.
[10] J.T. Gostick, M.W. Fowler, M.A. Ioannidis, M.D. Pritzker, Y.M. Volfkovich, A. Sakars, J. Power Sources 156 (2006) 375–387.
[11] E.C. Kumbur, K.V. Sharp, M.M. Mench, J. Electrochem. Soc. 154 (2007) B1295–B1304.
[12] M.S. Valavanides, A.C. Payatakes, Adv. Water Resour. 24 (2001) 385–407.
[13] B. Markicevic, N. Djilali, Phys. Fluids 18 (2006) 033101.
[14] M.R. Rasaei, M. Sahimi, Comput. Geosci. 13 (2009) 187–214.
[15] C.A. Aggelopoulos, C.D. Tsakiroglou, Geoderma 148 (2008) 25–34.
[16] I. Fatt, Trans. AIME 207 (1956) 164–181.
[17] R. Lenormand, E. Touboul, C. Zarcone, J. Fluid Mech. 189 (1988) 165–187.
[18] D. Or, Adv. Water Resour. 31 (2008) 1129–1136.
[19] M. Prat, Int. J. Multiphase Flow 19 (1993) 691–704.
[20] R. Lenormand, C. Zarcone, Phys. Rev. Lett. 54 (1985) 2226–2229.
[21] D. Wilkinson, J.F. Willemsen, J. Phys. A 16 (1983) 3365–3376.
[22] G.N. Constantinides, A.C. Payatakes, AIChE J. 42 (1996) 369–382.
[23] J.T. Gostick, M.W. Fowler, M.D. Pritzker, M.A. Ioannidis, L.M. Behra, J. Power Sources 162 (2006) 228–238.
[24] B. Markicevic, A. Bazylak, N. Djilali, J. Power Sources 163 (2007) 706–717.
[25] A. Bazylak, V. Berejnov, B. Markicevic, D. Sinton, N. Djilali, Electrochim. Acta 53 (2008) 7630–7637.
[26] J.H. Nam, M. Kaviany, Int. J. Heat Mass Transfer 46 (2003) 4595–4611.
[27] K.J. Lee, J.H. Nam, C.J. Kim, Electrochim. Acta 54 (2009) 1166–1176.
[28] K. Tüber, D. Pocza, C. Hebling, J. Power Sources 124 (2003) 403–414.
[29] N. Pekula, K. Heller, P.A. Chuang, A. Turhan, M.M. Mench, J.S. Brenizer, K. Ünlü, Nucl. Instrum. Methods Phys. 542 (2005) 134–141.
[30] S. Litster, D. Sinton, N. Djilali, J. Power Sources 154 (2006) 95–105.
[31] M. Rebai, M. Prat, J. Power Sources 192 (2009) 534–543.
[32] M. Blunt, M.J. King, H. Scher, Phys. Rev. A 46 (1992) 7680–7699.
[33] J. Bear, Dynamics of Fluids in Porous Media, Dover Publications, Inc., 1988.